PROCEEDINGS OF SCIENCE

Track and vertex reconstruction performance of the ATLAS detector

Götz Gaycken, on behalf of the ATLAS Collaboration [a,*]

[a] *University of Oregon (US)*

During its third data taking period, the Large Hadron Collider provided record-breaking integrated and instantaneous luminosities, resulting in huge amounts of data being provided with numbers of interaction per bunch crossing significantly beyond initial projections. In spite of these challenging conditions, the ATLAS Inner Detector track reconstruction continued to perform excellently. In this contribution the algorithms used to reconstruct charged particles and primary vertices will be described. The software configuration used for the Run 3 data-taking period and its performance will be presented using data and simulated events. Additional track reconstruction passes, developed to improve the tracking capabilities in dedicated physics scenarios, will be discussed as well.

42nd International Conference on High Energy Physics
Jul 17 – 24, 2024
Prague, Czech Republic

[*] Speaker

In the Run 3 of the Large Hadron collider, the average number of interactions per bunch crossing (μ) increased from an average of 30 (Run 2) to an average of about 50 (Figure 1(a)). The impact on the track and vertex reconstruction time in ATLAS [1–3] is shown in Figure 1(b).When using the Run 2 reconstruction, the time to reconstruct inner detector tracks and vertices nearly triples from $\mu \simeq 30$ to 60. Since this is a major component of the total reconstruction time, every aspect of the track and vertex reconstruction had been reoptimised for Run 3 to reduce the total reconstruction time at large μ, as detailed in Reference [5]. A summary is given in the following.

1 The ATLAS Inner detector

The ATLAS inner detector is immersed in a 2 T axial magnetic field and allows to reconstruct charged particle trajectories up to a pseudo rapidity ($|\eta|$) of 2.5. It is composed of $4(2 \times 3)$ silicon pixel layers in the barrel(positive and negative endcaps), where the innermost layer in the barrel (IBL) was added before Run 2. The Pixel detector is surrounded by the semiconductor tracker (SCT) which is composed of $4(2 \times 9)$ layers of double sided silicon strip sensors with a small stereo angle in the barrel(endcaps). At the very outside and covering an $|\eta|$ range up to 2, there are stacks of drift tubes which compose the transition radiation tracker (TRT). The TRT drift tubes had been filled originally with Xenon, now some are filled with Argon.

2 Overview of the inner detector track reconstruction

The first step of the track reconstruction is the *seed finding*. Seeds are constructed from triplets of pixel clusters of different layers, or triplets of SCT space points, where the latter is computed using compatible clusters found on the opposing sensor sides. The triplets have to fulfill certain momentum and impact parameter requirements. They are the basis for trajectory candidates.

Then *roads* are build along the seed, where the roads define which sensors are considered to search for compatible clusters to extend the seed trajectory. The trajectories are constructed by applying the Kalman filtering formalism, where in each step the trajectory is extended by clusters from consecutive detector layers.

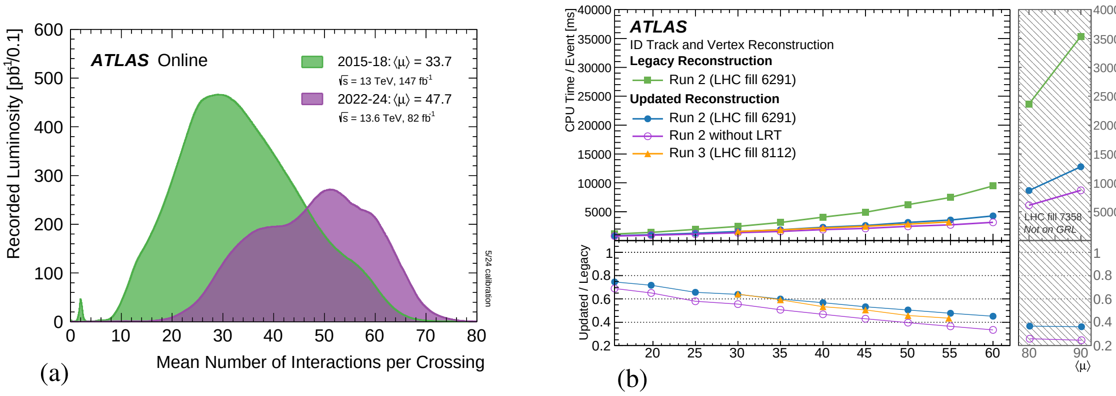

Figure 1: (a) distribution of the average interactions per bunch-crossing in ATLAS during the LHC Run 2 (2015-18), and the beginning of Run 3 (2022 - first half of 2024) [4]. (b) Inner detector track and vertex reconstruction time as a function of the average interactions per bunch crossing [5].

Although unused seeds are only considered for additional trajectories if there is no trajectory which incorporates all the measurements a seed is composed of, it still can happen that mostly identical trajectories are constructed. Such duplicates are removed in the *ambiguity resolution* step. During this step an artificial neural network is used to estimate the number of particles which traversed pixel clusters, as well as the exact positions where the cluster was traversed, and the associated uncertainties. Trajectories are scored according to hit, hole and shared hit counts and then depending on the score kept or discarded. Then, a global χ^2 fit is performed for all remaining trajectories to improve the resolution of their track parameters.

After that the tracks reconstructed from the silicon detector measurements are extrapolated towards the TRT. The TRT measures the drift time towards the wire at the centre of each tube, which constrains the hit positions on *drift circles* around the wires. The trajectory is extended by adding compatible drift circles and the resolution of the final trajectory is improved by a global χ^2 fit.

The first track reconstruction pass is followed by an *outside-in* pass, which is in particular of relevance for tracks which start late in the detector, e.g. tracks from converted photons. It is limited to regions of interest identified by calorimeter clusters. It starts from segments identified in the TRT and otherwise is similar to the *inside-out* pass.

3 Reoptimisation of the inner detector track reconstruction

For Run 3, every step of the inner detector track reconstruction has been retuned and re-optimised. The criteria of the various steps were harmonised, to minimise computations discarded by subsequent steps. The improvements in the reconstruction time are shown relative to the Run 2 reconstruction in Figure 2.

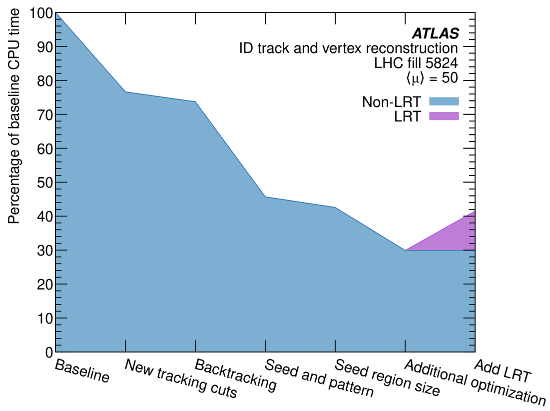

Figure 2: Evolution of the track reconstruction time for data relative to the Run 2 reconstruction [5].

The time was significantly reduced by tightening impact parameter cuts, requiring more Pixel or SCT hits per track, and by refining the regions of interest to seed the outside-in pass. The seed criteria were better adjusted for the subsequent steps, most notable tighter impact parameter cuts, which depend on how well clusters align with a straight line in the plane parallel to beam-axis, and the requirement of a forth confirmation pixel cluster or SCT space point. Finally general code optimisations were applied, and cuts on TRT drift circles were tightened. The improvements allowed to add an extra track reconstruction pass (LRT) to construct tracks which start at large radius while staying within the targeted CPU budget.

With all the improvements in place, the track reconstruction efficiency, shown in Figure 3(a), remained in most parts of the phase space within 1% of the efficiency obtained with the Run 2 reconstruction. At low p_T the efficiency drop is still smaller than 4%.

The number of tracks, shown in Figure 3(b), is expected to increase linearly with μ. Its deviation from a linear extrapolation is a measure of the number of falsely reconstructed tracks i.e.

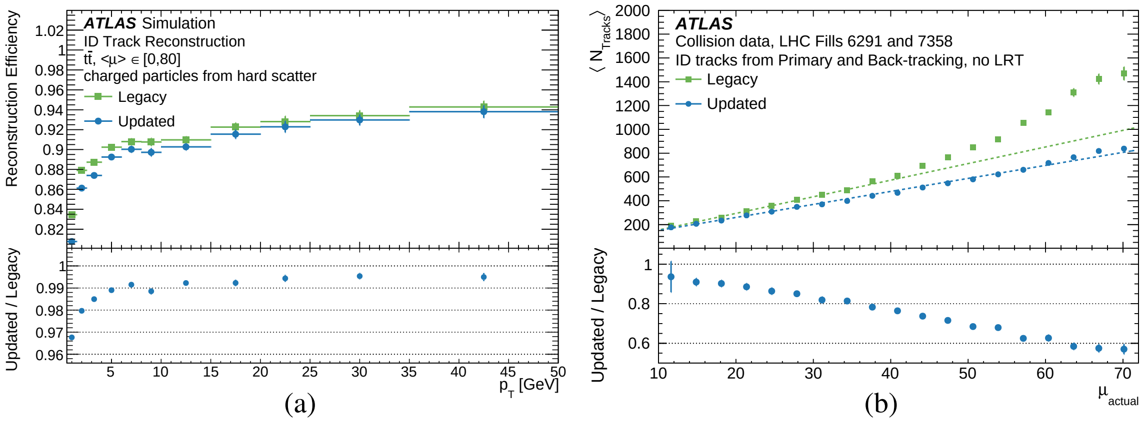

(a) (b)

Figure 3: (a) Comparison of the track reconstruction efficiency in $t\bar{t}$, for a μ distribution between 0 and 80 as a function of the momentum in the transverse plane to the beam-axis obtained with the Run 3 and Run 2 track reconstruction. (b) Comparison of the average number of tracks as a function of the number of interactions per bunch crossing (μ) in data, which is expected to increase linearly with μ. The deviation from the linear extrapolation is a measure of tracks reconstructed from arbitrary measurements (*fake tracks*) [5].

tracks which do not originate from a charged particle but arbitrary measurements (*fake* tracks). The Run 2 reconstruction yields more tracks than the Run 3 reconstruction due the higher reconstruction efficiency, but for $\mu \gtrsim 40$ also the fake track fraction increases significantly. It starts to outweighs the efficiency gain over the Run 3 reconstruction at a μ of 50. In contrast, the Run 3 track reconstruction has a negligible fake rate up to a μ of 70.

According to the projections, both the Pixel and SCT detector modules have enough head-room to account for the expected radiation damage for the remainder of Run 3. Thus, it should be possible to maintain the track reconstruction efficiency throughout Run 3 without loosening the track quality requirements. Figure 4 shows as an example the hit efficiency for one SCT silicon sensor as a function of the applied high voltage for several years from 2015 to 2024. The impact of the radiation damage is clearly visible, but the high voltage can still be increased enough to maintain maximal hit efficiency.

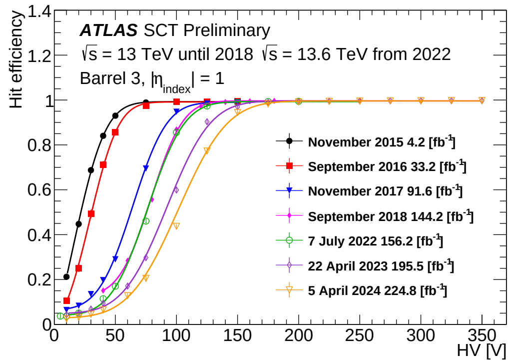

Figure 4: Hit efficiency for one SCT sensor as a function of the applied high voltage (HV) measured in different years from 2015 to 2024 [6].

4 Large radius tracking

In addition to improvements to the track reconstruction time, also the general memory consumption was reduced. This was achieved by moving from *multi processing*, to *multi threading* [7]. In the multi processing model a job is forked into one process per available CPU core after the first event is processed. In this model memory needed for static resources is shared. However, resources to e.g. model detector conditions, or memory needed for monitoring purposes change during the event processing, and less and less memory is shared. In the multi threading model, *threads* instead of processes are started for each available CPU core. Threads share the same memory space. Thus, also non-static resources are shared to a large degree and memory is used much more economically.

The memory savings and the reduction of the track reconstruction time allowed to add a track reconstruction pass for tracks which start at large radius [8]. The algorithm is very similar to the primary track reconstruction pass, but since the tracks start late in the detector and may not have 3 pixel hits on tracks, it only uses SCT seeds to start the track finding. Such tracks are mostly relevant for searches for new physics, and typically have large transverse momenta, therefore corresponding cuts are tightened. The impact parameter cuts, on the other hand, are significantly wider allowing the coverage of a phase space not covered by the main pass. Figure 5 shows the track reconstruction efficiency as a function of the production radius of the associated charged particle. The reconstruction efficiency of the inside-out and outside-in passes level off quickly. The large radius tracking pass starts to dominate already at a production radius of ∼ 2.5 cm.

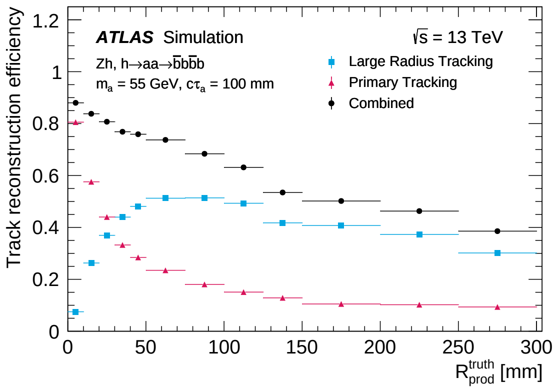

Figure 5: Track reconstruction efficiency for the primary, combined inside-out and outside-in track reconstruction pass, and the large radius track reconstruction pass as a function of the production radius of the associated charged particle [8].

5 Improved vertex finding

The original primary vertex finder, the *iterative vertex finder* (IVF), was developed for a small number of interactions per bunch crossing. For Run 3, it was replaced by the *adaptive multi vertex finder* (AMVF) provided by the Acts package [10].

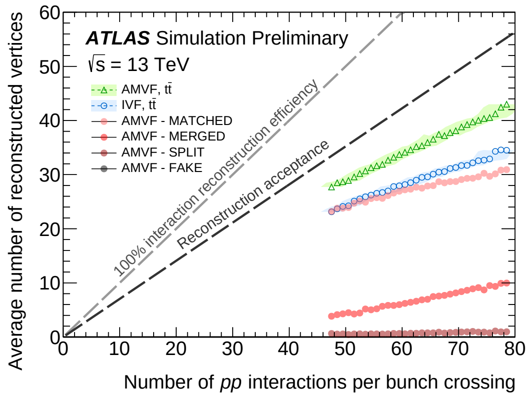

Figure 6: Average number of reconstructed primary vertices per event as a function of μ for different algorithms, IVF (Run and Run 2) and AMVF (since beginning of Run 3). For AMVF the vertices are also sub-categorised according to the true vertices the associated particles originate from [9].

It uses a Gaussian track density seed finder and then uses an adaptive Kalman fitter with deterministic annealing and beam spot constraints. An additional important ingredient is a vertex seed constraint, which prevents primary vertices from different seeds to be pulled towards the dominant vertices. Figure 6 shows the number of vertices as a function of μ. The AMVF has a higher vertex finding efficiency than the original IVF. Still, 12(19)% of the vertices at $\mu = 50(80)$ are not reconstructed as individual vertices. The number of true vertices reconstructed as more than one vertex is negligible, and so is the number of vertices constructed predominantly from tracks not originating from a single vertex (*fake* vertices).

As an alternative a vertex finder originally developed for LHCb was investigated [11]. It uses a convolutional neural network (CNN) for seed finding and to estimate the position along the z-axis (beam axis). The CNN uses as inputs moments of the track density distribution, and outputs a vertex probability as a discrete function of the z-coordinate. It significantly increases the vertex finding efficiency. Studies are ongoing on data which differs in detector alignment and noise amongst others compared to the datasets used for the training.

6 Summary

The entire inner detector track and vertex reconstruction chain used for the Run 3 reconstruction has been retuned and reoptimised for the conditions of Run 3, for which in particular the average number of interactions per bunch crossing increased from about 30 (Run 2) to 50. The processing time at $\mu \simeq 60$ was reduced by more than a factor of two, without sacrificing the track reconstruction efficiency. The efficiency is within 1% of the track reconstruction efficiency of Run 2 for the majority of the phase space. For tracks with low transverse momentum it is still within 4%. The projections suggest that this track reconstruction efficiency can be maintained throughout Run 3. Moreover the reduced processing time and the more economical usage of memory in the new multi threaded processing model, allowed for an additional tracking pass to construct tracks which are produced at large radius, and which allow for a considerable expansion of the ATLAS search program.

References

[1] ATLAS Collaboration, *JINST* **3** (2008) S08003.

[2] ATLAS Collaboration, CERN-LHCC-2010-013, ATLAS-TDR-19, 2010. URL: https://cds.cern.ch/record/1291633.

[3] ATLAS Collaboration, CERN-LHCC-2012-009, ATLAS-TDR-19-ADD-1, 2012. URL: https://cds.cern.ch/record/1451888.

[4] ATLAS Collaboration, 2024. URL: https://twiki.cern.ch/twiki/bin/view/AtlasPublic/LuminosityPublicResultsRun3.

[5] ATLAS Collaboration, *Comput. Softw. Big Sci.* **8** (2024) 9 [2308.09471].

[6] ATLAS Collaboration, IDET-2024-001, 2024. URL: https://atlas.web.cern.ch/Atlas/GROUPS/PHYSICS/PLOTS/IDET-2024-001/.

[7] ATLAS Collaboration, ATL-SOFT-PUB-2021-002, 2021. URL: https://cds.cern.ch/record/2771777.

[8] ATLAS Collaboration, *Eur. Phys. J. C* **83** (2023) 1081 [2304.12867].

[9] ATLAS Collaboration, ATL-PHYS-PUB-2019-015, 2019. URL: https://cds.cern.ch/record/2670380.

[10] P. Gessinger et al., *EPJ Web Conf.* **245** (2020) 10003.

[11] ATLAS Collaboration, ATL-PHYS-PUB-2023-011, 2023. URL: https://cds.cern.ch/record/2858348.